Correlation between Elemental Distribution and Susceptibility Change in Intracerebral Hemorrhagic Stroke

W. Zheng[1], E. M. Haacke[1], and H. Nichol[2]
[1]Radiology, Wayne State University, Detroit, Michigan, United States, [2]Department of Anatomy and Cell Biology, University of Saskatchewan, Saskatoon, Saskatchewan, Canada

Introduction. Both T2* weighted imaging (T2*WI) and susceptibility weighted imaging (SWI) are sensitive to local susceptibility change and widely used in similar clinical applications like stroke, traumatic brain injury and microbleeds [1]. Here in our recent work, we introduced the quantitative elemental mapping technique, synchrotron Rapid Scanning X-ray Fluorescence (RS-XRF) [2] to investigate how major elements (Fe, Ca and Zn) are related to the susceptibility change in intracerebral hemorrhagic stroke. At the same time, we looked at the pros and cons of quantitative T2* and susceptibility mapping (SWIM) in representing the iron-related susceptibility changes.

Methods. Three formalin fixed coronal sections of human cadaveric brains (four hemispheres) were obtained from the Human Brain and Spinal Fluid Resource Center (HSB), Los Angeles, CA under university ethics approval. For the first brain, the cause of death was hemorrhage (10 days after stroke). The second brain had both hemorrhage and multiple sclerosis but detailed stroke information was not available. The third brain had ischemic stroke three years before death (data not shown). Hemispheres were embedded in gelatin for MRI and then sectioned for XRF scans.

MR Images were collected on a 3T Siemens Verio system using a T2* weighted multi-echo SWI sequence with 11 echoes (TR=40ms, FA=15°). The images were acquired with resolution 0.5mmx0.5mm in phase and readout directions and 0.7mm in slice direction (coronal) with a bandwidth of 465Hz/pixel, a field-of-view of 256mm x 192mm resulting in 512 x 384 matrix for 40 slices. The shortest echo time was 5.68ms with a 2.57ms incremental for the other 10 echoes. MR phase images were first filtered by a 64x64 high pass filter and then processed using the SWIM algorithm [3] to create susceptibility maps using software SPIN (Signal Processing in NMR, Detroit, MI, USA). T2* maps were calculated from multi-echo SWI images in SPIN. FLAIR images were also collected in coronal direction with TR=9000ms, TE=74ms and 1mmx1mmx1mm resolution with matrix size 256x192x32.

The region of interest was identified in MR images; and the brain hemispheres were sectioned for synchrotron imaging. RS-XRF images were acquired at wiggler beam line 10-2 at the Stanford Synchrotron Radiation Lightsource (SSRL). The samples were mounted on a set of motorized stages oriented at 45° to the incident beam. The incident beam (12 keV) passing through a tantalum aperture produced a 100 μm x 100 μm spot on the sample which was raster-scanned in the beam using a dwell time of 15ms/point. Fluorescent energy windows were centered for Fe (6.21 - 6.70 keV), Ca (3.52 3.96 keV), Zn (8.38 - 8,98 keV) as well as all other biologically interesting elements, scatter and total incoming counts. The data were quantified in μg Fe/g w/w tissue using Sam's Microanalysis kit (http://ssrl.slac.stanford.edu/~swebb/smak.html) as previously described (4).

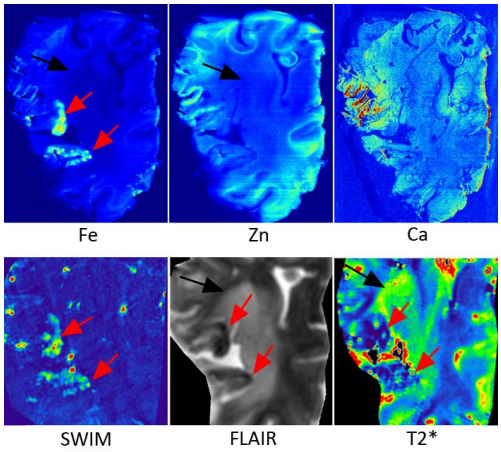

Fig.1. Correlation between XRF elemental maps (Fe, Zn and Ca) and MR imaging (SWIM, FLAIR and T2* map) in a cadaver brain 10 days after stroke.

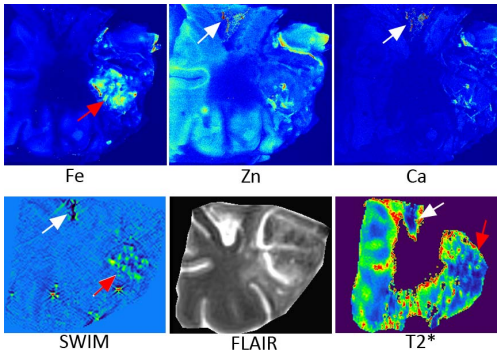

Fig.2. Correlation between XRF elemental maps (Fe, Zn and Ca) and MR imaging (SWIM, FLAIR and T2* map) for the second brain. Stroke information is not available but necrosis was evident.

Results. In the brain with death 10 days after stroke (Fig.1), XRF elemental maps of the ICH (red arrows) show the expected elevated Fe but this was accompanied by Zn depletion. Ca and Fe were not co-localized in the lesion. Susceptibility changes in SWIM accurately depicted Fe location caused by hemorrhage according to the XRF Fe map. The region with elevated iron was visualized in the T2* map but SWIM provided superior spatial and quantitative resolution of Fe. The location of hemorrhage was also clearly shown in FLAIR. All the elements in XRF maps were depleted in a region of infarct (black arrows) and this was also seen in ischemia in the absence of hemorrhage in a 3rd brain (data not shown). The infarct is clearly visualized in both FLAIR and T2* map but not seen in SWIM and this may be explained by the absence of iron.

In the second brain sample with old stroke, a necrotic region (red arrows in Fig.2) with high levels of iron shown in the XRF Fe map is clearly visualized in SWIM. The region of necrosis also shows spots that are rich in Zn and Ca with Zn co-localizing with Ca. This high Ca information was captured by both SWIM and T2* map. But T2* failed to differentiate it from Fe in term of T2* shortening. The T2* map again was less specific in visualization of iron related susceptibility changes than SWIM.

Conclusion. In this study, we gained some preliminary knowledge of elemental distribution associated with fresh hemorrhage and old hemorrhage. With this knowledge, we find SWIM is superior to T2* for imaging iron in hemorrhage and can differentiate Ca from Fe. SWIM is capable of imaging both new hemorrhage and necrotic tissue containing old hemorrhages, but not capable of capturing ischemic lesions unrelated to hemorrhage. Our findings demonstrate that SWIM and T2* map complement each other and can provide more specific and accurate spatial and chemical information in ICH and other Fe/Ca related susceptibility changes.

Acknowledgments. The authors would like to thank Sam Webb at the Stanford Synchrotron Radiation Lightsource and Angela Auriat at the Dept. of Neurosurgery, Stanford University for their help in collecting XRF data. This work is supported by Heart and Stroke Foundation of Canada (HSFC) and the Canadian Institutes of Health Research (CIHR) - Institute of Circulatory and Respiratory Health, Clinical Imaging Initiative (FRN - 99472) to HN.

References: (1) Haacke et al. AJNR, 30:19, 2009. (2) Popescu et al. Phys Med Biol, 54:651, 2009. (3) Haacke et al. JMRI, 32:663, 2010. (4) Hopp et al. JMRI, 31:1346, 2010.